EMTP Modeling of a Triggered-Lightning Strike to the Phase Conductor of an Overhead Distribution Line

Carlos T. Mata, *Student Member, IEEE*, Mark I. Fernandez, Vladimir A. Rakov, *Senior Member, IEEE*, and Martin A. Uman, *Fellow, IEEE*

***Abstract*—A triggered-lightning experiment and EMTP modeling of that experiment are used to study the responses of a two-conductor overhead power line to a direct lightning strike. The experiment was conducted at the International Center for Lightning Research and Testing (ICLRT) at Camp Blanding, FL. The lightning was artificially initiated (triggered) from a natural thundercloud using the rocket-and-wire technique, and its current was directed to the phase conductor. EMTP modeling of the line behavior yields results that are generally consistent with the measurements.**

***Index Terms*—ATP-EMTP, grounding electrodes, lightning, MOV arresters.**

I. Introduction

THE INTERNATIONAL Center for Lightning Research and Testing (ICLRT) is located at Camp Blanding, Florida, approximately midway between Gainesville and Jacksonville. The ICLRT is an outdoor facility that occupies about 100 acres and is used for triggering lightning artificially from natural overhead thunderclouds using the rocket-and-wire technique [1], [2]. An overview of the ICLRT facility at the time of the lightning strike considered in this paper is shown in Fig. 1. The facility included an unenergized test power line supported by fifteen poles. The line had two vertically stacked conductors, the top conductor being referred to as the phase conductor and the bottom conductor as the neutral. In the configuration considered here, a total of four arresters were installed on the line, at poles 1, 9, 10, and 15 (see Fig. 1), between the phase and the neutral conductors, and the neutral of the line was grounded at these four poles. In one of the 1996 tests (Event 9621), the lightning current was directed to the phase conductor of the line between poles 9 and 10. During this particular event the arrester at pole 10 failed. Video records show that the failure occurred during the initial stage (that is prior to the first return stroke) of the triggered-lightning discharge. The initial stage typically involves a current flow of the order of 100 A for hundreds of milliseconds [3]. The line was instrumented to measure the voltages and currents at various points including voltages across and currents through arresters, and currents to ground. The interaction of lightning with the overhead line is modeled using EMTP. Model predictions are compared to measurements.

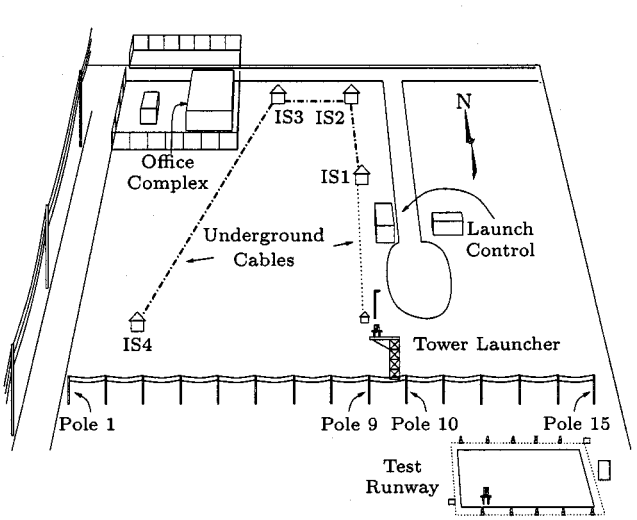

Fig. 1. Overview of the ICLRT at Camp Blanding, FL in 1996.

II. Experiment

In this section we give more details on the characteristics of the transmission line, including arresters and grounding, and describe the measurement locations and the measurement equipment used.

A. Configuration of the Line

The line is approximately 740 m long and is terminated at both ends in its characteristic impedance of about 500 Ω. The distance between poles varied from 47 to 73 m. Both the phase and the neutral were "Azusa," seven-strand conductors. They were mounted on insulators having a critical flashover voltage (CFO) of 500 kV and separated by 1.8 m. MOV arresters installed at poles 1, 9, 10, and 15 were 10-kV distribution arresters. Grounding of the line's neutral at these four poles was accomplished by means of 24-m cooper vertically-driven rods. The low-frequency, low-current grounding resistance of the ground rods was measured on several occasions using the fall-of-potential method. The measured grounding resistances as of May 1996 were 56, 26, 50, and 41 Ω for ground rods at poles 1, 9, 10 and 15, respectively. Although long-term variation of grounding

Manuscript received April 30, 1999; revised February 8, 2000. This research was supported in part by EPRI (Project Manager R. Bernstein) and by NSF Grants ATM 9415507 and 9726100.

The authors are with the Department of ECE, University of Florida.

Publisher Item Identifier S 0885-8977(00)10306-1.

TABLE I
V–I CHARACTERISTIC OF THE 10-kV MOV ARRESTERS BASED ON AN 8/20 μs WAVE

Discharge Voltage kV	Discharge Current kA
29.7	1
31.6	2.5
32.5	5
36.4	10
39.7	20

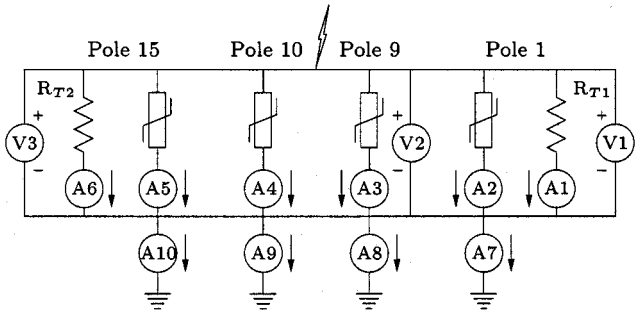

Fig. 2. Test system configuration and measurement locations.

resistance should be small, short-term variation could be significant due to sporadic rainfall in Florida, particularly during the summer months [4]. The V–I characteristic of the 10-kV arresters is shown in Table I.

B. Instrumentation and Measurement Locations

The currents were measured at each arrester and at each ground rod with 16.5-mΩ current viewing resistors (shunts) and were recorded with Macrodyne Lightning Transient Recorders (LTR's). The voltages were measured between the phase and neutral conductors at the arrester locations (except for Pole 10 where no measurements are available due to the arrester failure at this pole) with 400-kV resistive voltage dividers and were recorded with Nicolet Pro 90 digitizing oscilloscopes at a 10 Mhz sampling rate. These oscilloscopes were housed in the Launch Control trailer (Fig. 1) and recorded the output signals of the voltage dividers remotely via Nicolet Isobe 3000 fiber optic links, each composed of an Isobe transmitter, a fiber optic cable, and an Isobe receiver. The total triggered-lightning current was measured at the rocket launching unit with a 1-mΩ shunt and three current transformers (CTs). Multiple sensors were used at the launcher to increase the dynamic range of the measurements and for redundancy. The outputs of the CTs were monitored by LTR's with three different ranges: 13, 28, and 50 kA. Locations of current (A) and voltage (V) sensors on the line are shown in Fig. 2.[1]

III. EMTP MODELING

The EMTP simulations were performed for two models of the system. In the first, the simpler model, the line was represented by a distributed R-L-C circuit with the skin effect and finite ground conductivity being neglected, the ground rods were modeled by resistors, and the leads connecting the neutral to ground rods (ground leads) were treated as short circuits. In the second, more complex model, frequency dependent line parameters (considering an imperfect ground and the skin effect [6]) and representation of the ground leads and the ground rods as distributed circuits were used. In both models, the MOV arresters were simulated by nonlinear elements such as to reproduce the V–I characteristic given in Table I. The failed arrester at Pole 10 was represented by a resistor whose value was selected by trial and error to achieve the best match between model predictions and measurements.

[1]For a detailed description of the experiment setup, and the instrumentation used, see [4] and [5].

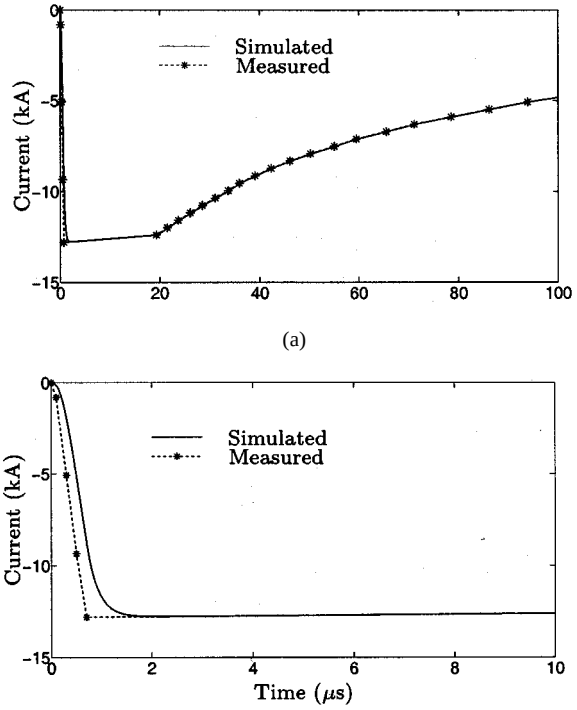

(a)

(b)

Fig. 3. Total lightning current versus time waveforms: a) on 100 μs and b) on 10 μs time scales.

A. Lightning Current

A type 1 (user defined) current source is employed in this simulation [6]. The LTR record ($\pm$13 kA range) of the total triggered-lightning current was up-sampled (using a linear interpolation algorithm) and then filtered by a first order Butterworth digital filter with a cutoff frequency of 700 kHz to smooth out the discontinuities in the waveform. These discontinuities are a result of LTR's limited vertical resolution. The waveform of the total lightning current (LTR record) and the current source used in the simulation are shown in Fig. 3 on 100 μs and 10 μs time scales.

B. Transmission Line

As noted above, two overhead line models were used in the simulation. In both models, the overhead line was divided into four sections (Fig. 4): pole 1 to pole 9 (391 m), pole 9 to the strike point (24.6 m), strike point to pole 10 (24.6 m), and pole 10 to pole 15 (298 m).

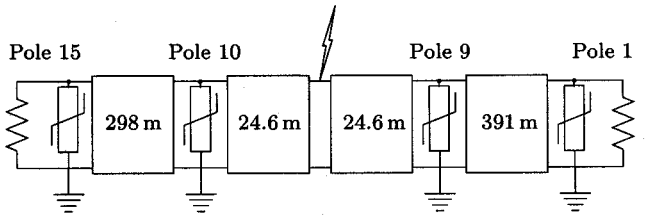

Fig. 4. Transmission line sections used in the model.

C. Arresters

Non-linear resistor type-92 is used to model the 10 kV arresters [6]. An EMTP subroutine (supporting program ARRDAT) was used to calculate the parameters required by the type 92 EMTP branch card. At Pole 10, the arrester failed during the initial continuous current that preceded the single return stroke of the flash, and its impedance (likely to be time varying) is unknown. The failed arrester at pole 10 was modeled as a constant resistance. From the EMTP modeling, this resistance determines the duration of operation of the other three arresters, but mainly the duration of operation of the arrester at pole 15. The failed arrester's resistance at pole 10 was adjusted so that the duration of the calculated discharge current through the arrester at pole 15 would match the duration of the measured arrester discharge current at this pole. This resistance was found to be approximately 0.1 Ω, although for a range from 1 mΩ to 1 Ω the system responses were not much different. If the value of the resistance is higher than 1 Ω, the overshoot seen in the measured voltage across the arresters is not reproduced. If the resistance is less than 1 mΩ, the model-predicted current through the arrester and the voltage across the arrester at Pole 15 differ significantly from the measurements.

D. Measurement of Voltage Across an Arrester

The measurement circuit consists of a voltage divider connected in parallel with the arrester. This configuration involves a loop formed by the arrester, voltage divider and wires, that connect the arrester to the phase and neutral conductors, as shown in Fig. 5. The arrester discharge current creates a time-varying magnetic flux that induces an unwanted voltage in the measuring loop. From Faraday's law, the distributed electromotive force (emf) induced in the loop is proportional to the derivative of the current with respect to time. Therefore, the voltage divider would "see" this emf in addition to the voltage across the arrester. The voltage "seen" by the voltage divider is then:

$$V_{\text{out}} \propto V_{phase} - V_{neutral} + k\partial I(t)/\partial t \qquad (1)$$

where

- V_{phase} is the voltage of the phase conductor with respect to ground,
- $V_{neutral}$ is the voltage of the neutral conductor with respect to ground and
- k is the proportionality constant, which can be viewed as the equivalent inductance of the loop.[2]

[2]The proportionality constant k was set at 6 μH so that the voltage spike at the beginning of the voltage waveform predicted by (1) would match the spike in the voltage waveform measured across the arrester at pole 9.

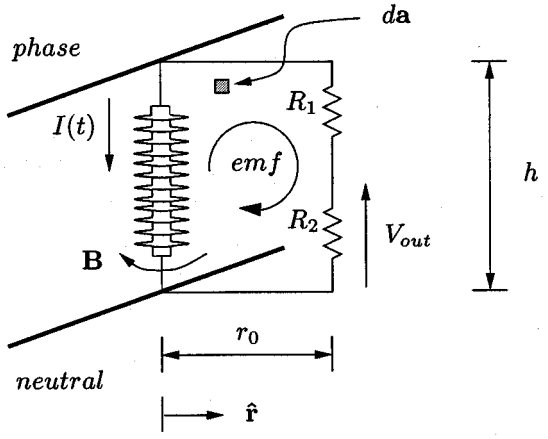

Fig. 5. Illustration of the measurement of voltage across the arrester.

E. Leads Connecting the Neutral to Ground Rods

In the first and simpler model, ground-lead impedances are neglected. In the second and more complex model, leads connecting the neutral to ground rods are represented as described bellow. The capacitance and inductance each per unit length of a vertical wire above ground in the absence of other conductors nearby are given by [7]:

$$C = \frac{2\pi\epsilon_0}{\ln(2h/r)}\ \text{[F/m]}; \qquad L = \frac{\mu_0}{2\pi}\ln(2h/r)\ \text{[H/m]} \qquad (2)$$

where h is the height above ground and r is the conductor's radius. The ground leads are 5.5 m long, and r is approximately 4.8 m. If we assume that the highest frequency component of the lightning current is approximately 1 MHz (which corresponds to a wavelength of 300 meters), then one pi section (lumped equivalent circuit) would be enough to model the ground leads. The highest frequency components in the system do not necessarily originate in the source. Nonlinear elements can generate frequency components that are higher than those present in the source. We found that the model-predicted waveforms would change if we increased the number of pi-sections representing each ground lead. The number of pi-sections was then incrementally increased until no significant difference in the computed voltage and current waveforms was seen. This led us to model the ground leads as distributed circuits consisting of 11 sections each.

F. Ground Rods

In the simpler model, ground rods are modeled as resistors. In the more complex model they are modeled as distributed R-L-C circuits, as shown in Fig. 6. It has been found by trial and error that 30 sections are sufficient for adequate modeling. The capacitance and inductance of the ground rod are given by [8]:

$$C = \frac{\epsilon_r l}{18\ln(4l/d)} \times 10^{-9}; \quad L = 2l\ln\left(\frac{4l}{d}\right) \times 10^{-7} \qquad (3)$$

where

- ϵ_r is the relative permittivity of the soil ($\epsilon_r = 10$ was used),
- l is the length (approximately 24 m), and
- d is the diameter of the ground rod (approximately 16 mm).[3]

[3]The capacitance and inductance in (3) are in [F] and [H], respectively.

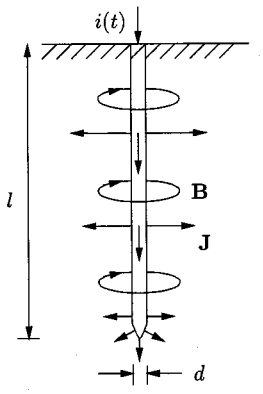

(a)

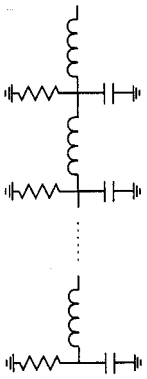

(b)

Fig. 6. Distributed-circuit model of ground rods: (a) Schematic representation of current flow and magnetic field lines; (b) equivalent circuit of the ground rod shown in (a). Adapted from [8].

The nonlinear resistance of the ground rod is usually expressed as a function of current through the rod [9]:

$$R_t(t) = \frac{R_0}{\sqrt{1 + i(t)/I_g}} \tag{4}$$

where R_0 is the measured low-frequency, low-current grounding resistance, $i(t)$ is the current through the rod, and I_g is given by:

$$I_g = \frac{E_0 \rho}{2\pi {R_0}^2} \tag{5}$$

In (5), E_0 is the critical electric field intensity (approximately 300 kVm [8]), and ρ is the ground resistivity. Using measured values of R_0, 26 to 56 Ω, $\rho = 4000$ Ω-m, we find that I_g is greater than 60 kA. Both measured and calculated currents to ground range from 2 to 8 kA, and hence they are considerably smaller than the computed value of I_g. As a result, the second term under the radical in (4) is negligible compared to unity and therefore $R_t \approx R_0$. Based on the above, we modeled ground rods as linear elements. Equations (4) and (5) imply that in our system the relatively high value of ρ, relatively low values of R_0, and relatively low values of currents through the rods make the ionization of soil in the vicinity of rods unlikely. However, (4) apparently does not account for electrical arcs that can develop radially from the ground rod along the ground surface and reduce the value of ground resistance with respect to R_0 [2].

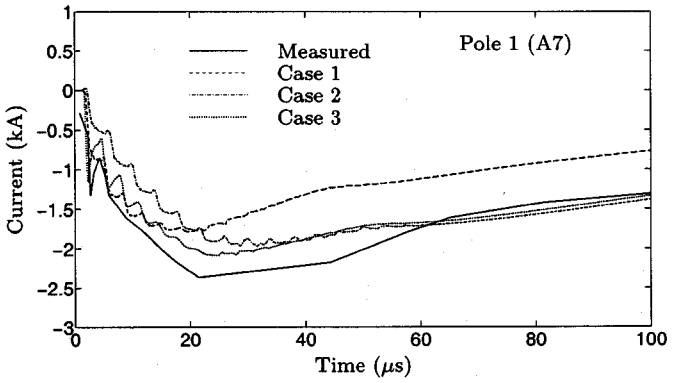

Fig. 7. Current to ground at pole 1 versus time displayed on a 100-μs scale.

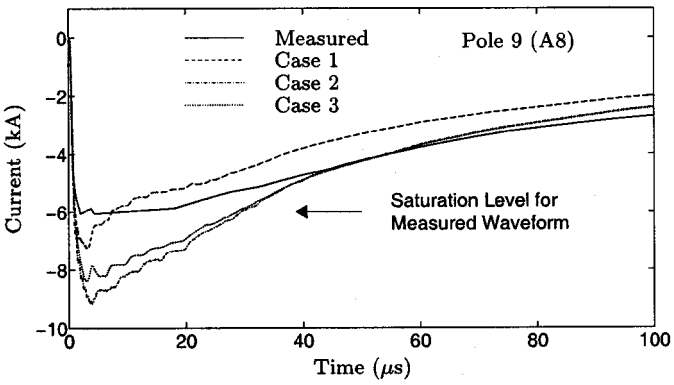

Fig. 8. Current to ground at pole 9 versus time displayed on a 100-μs scale.

IV. Results

The simulation was performed for three different cases:

Case 1) Simpler model with measured grounding resistances, 56, 26, 50, and 41 Ω, for poles 1, 9, 10, and 15, respectively.

Case 2) Simpler model with adjusted values of grounding resistances.[4] These values were 30, 13, 60, and 56 Ω for poles 1, 9, 10, and 15, respectively.

Case 3) Complex model using the adjusted values of grounding resistances from Case 2.

For Cases 1 and 2 only current waveforms are shown since the voltage waveforms are very similar to those for *Case 3.*

A. Currents to Ground: Cases 1, 2, and 3

The measured and calculated currents to ground at pole 1, shown in Fig. 7, are in good agreement. Model-predicted waveforms at poles 9, 10, and 15 (Figs. 8–10, respectively) for Case 1 show systematic difference of the order of 1 kA with respect to measured waveforms at later times. Overall, it seems that the system allows more current to be drained to ground at poles 1 and 9 than at poles 10 and 15. We assumed that the discrepancies are due to the lack of knowledge of the grounding resistances at the time of this experiment, and we adjusted these resistances

[4]The adjusted values of grounding resistances were obtained by running an optimization *open-loop* algorithm (using the Nelder–Mead simplex direct search method) in which EMTP was run from MATLAB to compare and minimize the area between the measured and calculated current-to-ground waveforms for Case 1.

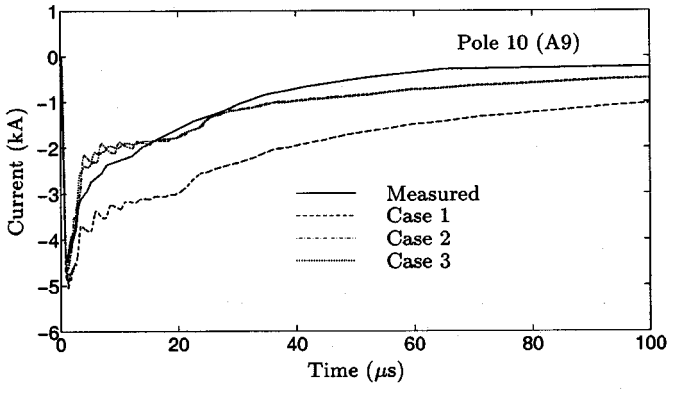

Fig. 9. Current to ground at pole 10 versus time displayed on a 100-μs scale.

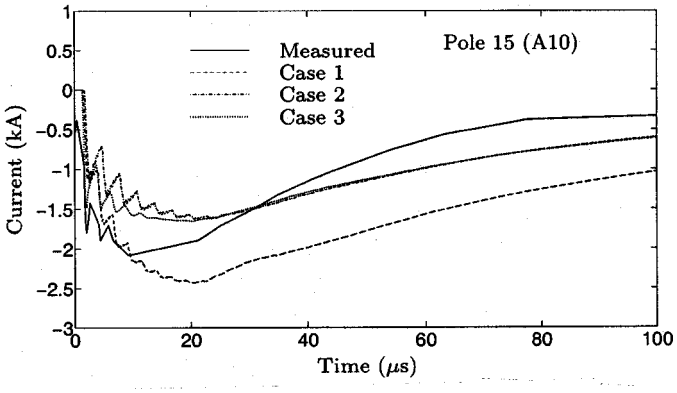

Fig. 10. Current to ground at pole 15 versus time displayed on a 100-μs scale.

so that the model-predicted and measured waveforms matched better (Case 2). Note that the distribution of currents to ground is mainly determined by the grounding impedances, and it is relatively insensitive to variations of the failed arrester's impedance at pole 10. The computed currents to ground for Case 3 are presented in the same figures (Figs. 7–10). For this last case, the measured and calculated current waveforms show better agreement than for Cases 1 and 2.

B. Arrester Discharge Currents: Cases 1, 2, and 3

Measured discharge currents through arresters at poles 1, 9, and 15, and calculated arrester discharge currents for Cases 1, 2, and 3, are shown in Figs. 11–13, respectively. Figs. 11 and 12 showing arrester currents at poles 1 and 9, respectively, suggest that the arresters operated for almost 10 μs longer than the model predicts. At pole 15 (Case 1), the arrester seems to operate for the same time duration as the model predicts. The initial spike (seen in the arrester currents at pole 1 and pole 15) might be the result of some high frequency current components that did not flow through either the failed arrester at pole 10 or the arrester at pole 9, and propagated toward poles 1 and 15. Overall, Case 3 reproduces better the measured current through the arresters than Cases 1 and 2.

C. Voltages Across the Arresters: Case 3

The calculated voltage with and without the magnetic coupling accounted for and the measured voltage across the arrester at pole 1 are shown in Figs. 14 and 15 on 100-μs and 10-μs

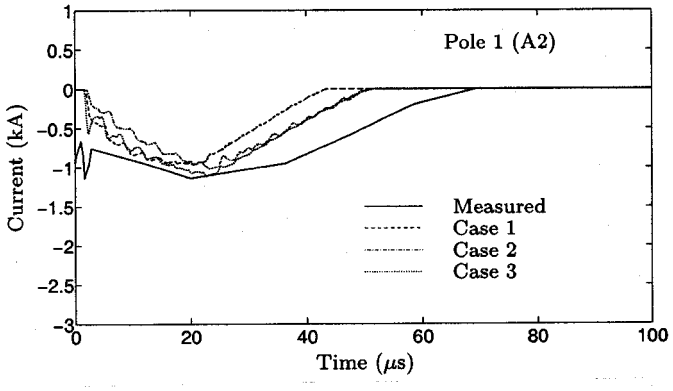

Fig. 11. Arrester discharge current at pole 1 versus time displayed on a 100-μs scale.

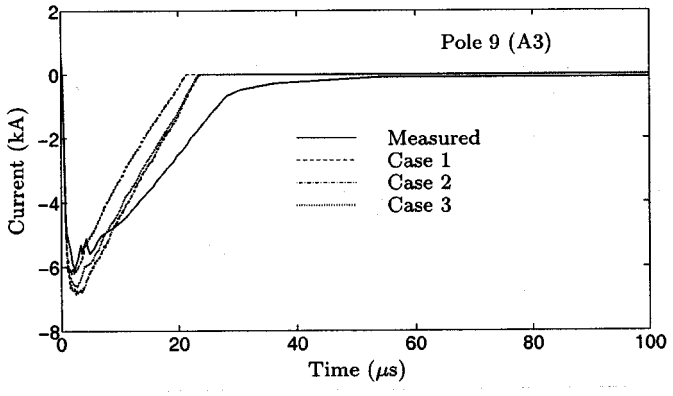

Fig. 12. Arrester discharge current at pole 9 versus time displayed on a 100-μs scale.

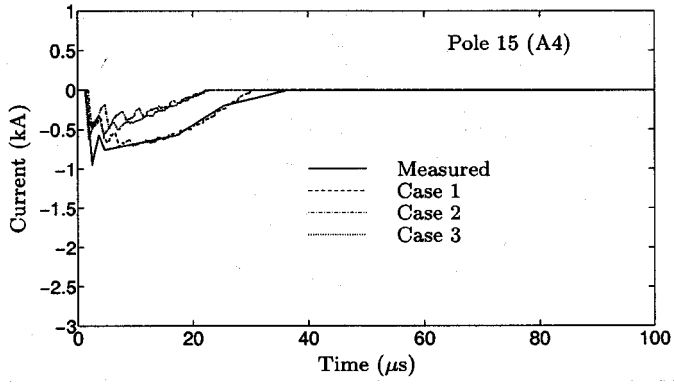

Fig. 13. Arrester discharge current at pole 15 versus time displayed on a 100-μs scale.

time scales, respectively. The measured waveform exhibits an initial negative spike of about 36 kV, a plateau at 25 to 19 kV lasting for approximately 65 μs, and an opposite polarity overshoot. Overall, the model-predicted waveforms and the measured waveform in Figs. 14 and 15 are similar. The calculated voltage with magnetic coupling modeled additionally exhibits fine structure (small pulsations superimposed on the plateau) and the initial spike observed in the measured voltage. Measured and calculated voltages at pole 9 are shown in Figs. 16 and 17. The measured voltage waveform at pole 9 shows an initial negative spike clamped at 95 kV (saturation level), followed

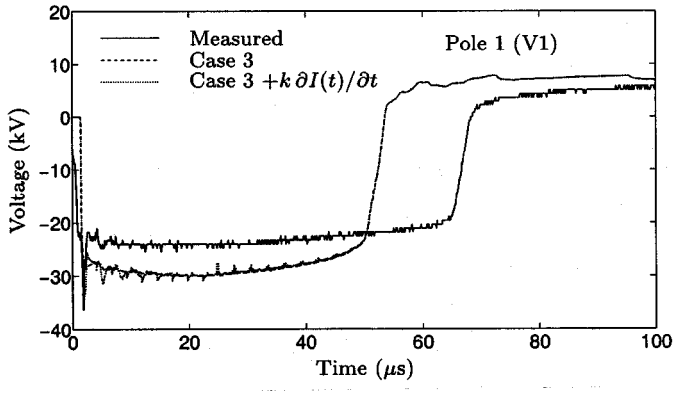

Fig. 14. Voltage across the arrester at pole 1 displayed on a 100-μs scale.

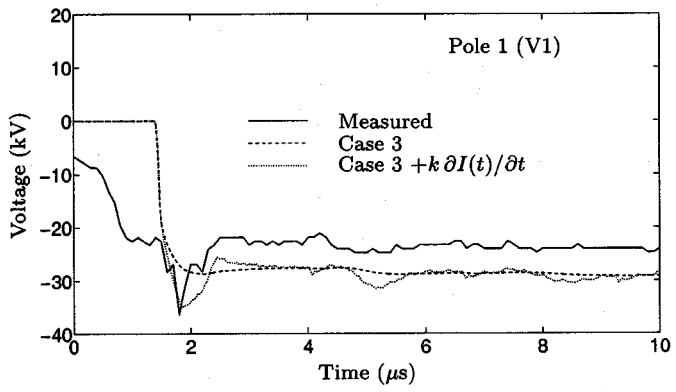

Fig. 15. Voltage across the arrester at pole 1 displayed on a 10-μs scale.

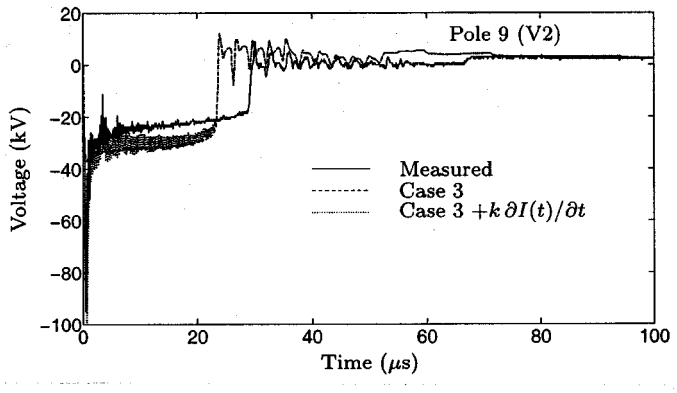

Fig. 16. Voltage across the arrester at pole 9 displayed on a 100-μs scale.

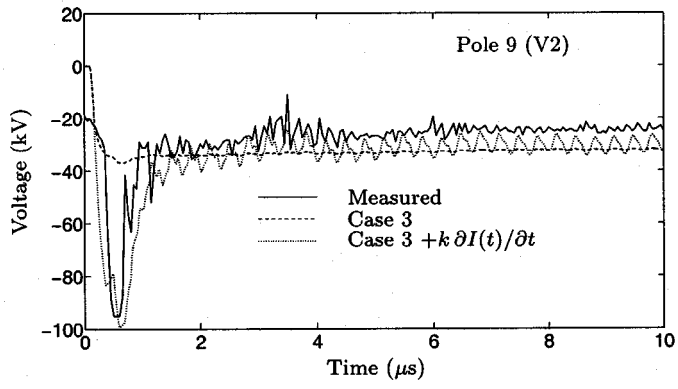

Fig. 17. Voltage across the arrester at pole 9 displayed on a 10-μs scale.

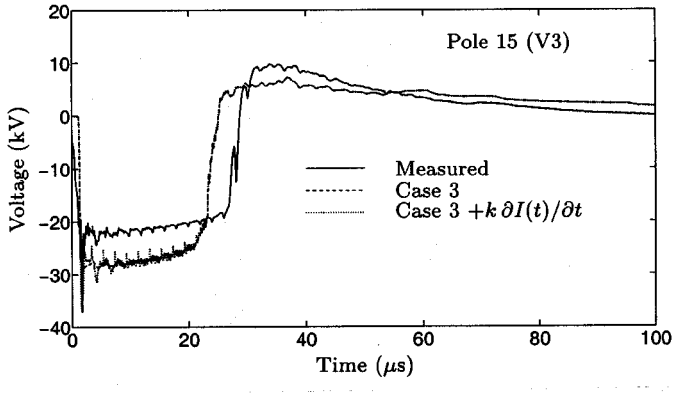

Fig. 18. Voltage across the arrester at pole 15 displayed on a 100-μs scale.

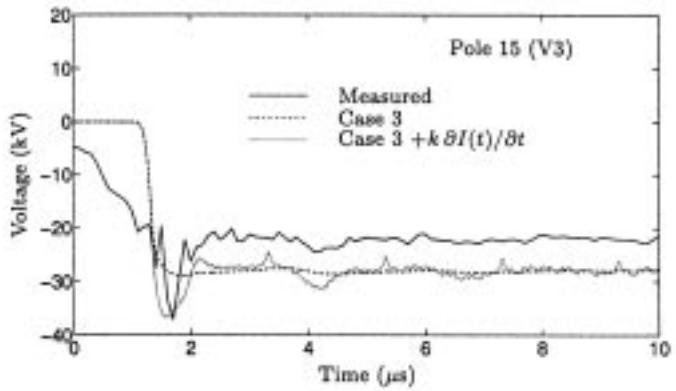

Fig. 19. Voltage across the arrester at pole 15 displayed on a 10-μs scale.

by damped oscillations superimposed on a plateau that decays slowly from 30 kV to 17 kV for about 29 μs. After the plateau, the voltage waveform crosses zero sharply and shows damped oscillations superimposed on a small positive overshot. The initial spike is reproduced when the calculated voltage across the arrester includes the contribution from magnetic coupling to the measuring circuit, as seen in Fig. 17. The proportionality constant k in (1) determines the magnitudes of the spike and the damped oscillations that follow. As noted earlier, a value of 6 μH has been adopted for k. Measured and calculated voltages at pole 15 are shown in Figs. 18 and 19. The measured waveform exhibits an initial negative spike of about 37 kV. This spike is followed by a plateau, that decays slowly from 22 kV to 18 kV for approximately 28 μs, and by an opposite polarity overshoot. Some small damped oscillations are superimposed on the plateau. The calculated voltage across the arrester with magnetic coupling modeled in Fig. 19 shows an initial negative spike of about 37 kV (the same as the measured value), followed by a plateau with small superimposed oscillations (also seen in the measurements). Overall, the calculated voltages with magnetic coupling modeled show better agreement with measurements than voltages computed for the other cases considered here.

V. Summary

EMTP simulations of lightning interaction with a power distribution system have been performed for different levels of complexity in the representation of the system, and the results are compared to measurements. The results are insensitive to the value of the resistance that is used to simulate the failed arrester at pole 10 in the range from 1 mΩ to 1 Ω. The impedance of the failed arrester at pole 10 appears to control (in conjunction with the three operating arresters) the rate of flow of charge from the phase conductor to the neutral conductor and to determine mainly the duration of operation of the three operating arresters. This impedance apparently has little effect on the distribution of currents flowing to ground via the four ground rods. The initial spikes in measured voltage across the arresters have been reproduced by considering magnetic coupling to the measuring circuit. Overall, measurements have been fairly well reproduced by both the simpler and the complex models. The complex model additionally reproduces the fine structure of the measured waveforms. The use of the complex model is recommended if more accurate and detailed waveforms are desired; otherwise the simple model is preferred. The measured distribution of currents to ground can be better reproduced by adjusting the values of grounding resistances within 50% of their measured values.

References

[1] M. A. Uman, V. A. Rakov, K. J. Rambo, T. W. Vaught, M. I. Fernandez, D. J. Cordier, R. M. Chandler, R. Bernstein, and C. Golden, "Triggered-lightning experiments at Camp Blanding, FL (1993–1995)," *Trans. IEE Japan, Special Issue on Artificial Rocket Triggered Lightning*, vol. 117-B, no. 4, pp. 446–452, 1997.

[2] V. A. Rakov, M. A. Uman, K. J. Rambo, M. I. Fernandez, R. J. Fisher, G. H. Schnetzer, R. Tottappillil, A. Eybert-Berard, J. P. Berlandis, P. Lalande, A. Bonamy, P. Laroche, and A. Bondiou-Clergerie, "New insights into lightning processes gained from triggered-lightning experiments in Florida and Alabama," *Journal of Geophysical Research*, pp. 14,117–14 130, 1998.

[3] D. Wang, V. A. Rakov, M. A. Uman, M. I. Fernandez, K. J. Rambo, G. H. Schnetzer, and R. J. Fisher, "Characterization of the initial stage of negative rocket-triggered lightning," *Journal of Geophysical Research*, vol. 104, pp. 2141–2150, 1999.

[4] M. I. Fernandez, C. T. Mata, V. A. Rakov, M. A. Uman, K. J. Rambo, M. V. Stapleton, and M. Bejleri, "Improved lightning arrester protection results, final results," Electric Power Research Institute (EPRI), Palo Alto, CA, Rep. TR-109 670-R1, Dec. 1998.

[5] M. I. Fernandez, "Responses of an unenergized test power distribution system to direct and nearby lightning strikes," Master's thesis, University of Florida, Gainesville, FL, 1997.

[6] Can-Am EMTP User Group, *Alternative Transients Program (ATP) Rule Book* Portland, OR, 1987–1998.

[7] E. M. Bazelyan, B. N. Gorin, and V. I. Levitov, "Physical and engineering foundations of lightning protection," in *Gidrometeoizdat*, St. Petersburg, Russia, 1978.

[8] A. F. Imece, D. W. Durbak, H. Elahi, S. Kolluri, A. Lux, D. Mader, T. E. McDermott, A. Morched, A. M. Mousa, R. Natarajan, L. Rugeles, and E. Tarasiewicz, "Modeling guidelines for fast front transients," *IEEE Trans. on Power Delivery*, vol. 11, no. 1, pp. 493–501, Jan. 1996.

[9] CIGRE Working Group 33-01 (Lightning) of Study Committee 33, Overvoltages and Insulation Coordination, *Guide to Procedures for Estimating the Lightning Performance of Transmission Lines* Paris, October 1991.

Carlos T. Mata received his Bachelor's degree from the "Universidad Simón Bolívar" (USB), Venezuela in 1993, his Master's from the University of Florida (UF) in 1997 and is working toward his Ph.D. degree at the University of Florida (UF). Mr. Mata is involved in the area of computer modeling of different lightning processes and responses of power distribution systems to direct and nearby lightning strikes. This work is part of large-scale studies at the International Center for Lightning Research and Testing (ICLRT) at Camp Blanding, FL. Since 1997 he has held a graduate research assistantship in the UF Lightning Research Laboratory. In 1998 Mr. Mata was awarded with the GAANN program (Graduate Assistance in Areas of National Need). He is author or co-author of four journal publications and five technical reports. Mr. Mata is a student member of the American Geophysical Union (AGU), the Institute of Electrical and Electronics Engineers (IEEE), and the Power Engineering Society (PES).

Mark I. Fernandez received his Bachelor's degree from Florida Institute of Technology (FIT), Melbourne in 1995, and his Master's degree from the University of Florida (UF), Gainesville in 1997. Mr. Fernandez was involved in magnetostatics and space plasma research as an undergraduate in the Department of Physics and Space Sciences at FIT. From 1995 to 1997, he held a graduate research assistantship in the UF Lightning Research Laboratory. He is author or co-author of five publications in reviewed journals, eleven published abstracts or conference proceedings, and four technical reports. Mr. Fernandez is a member of the American Geophysical Union.

Vladimir A. Rakov is Professor of the University of Florida's (UF) Department of Electrical and Computer Engineering. He is the author or co-author of over 30 patents and over 180 papers and technical reports on various aspects of lightning, with over 60 papers being published in reviewed journals. Dr. Rakov received the Master's and Ph.D. degrees from Tomsk Polytechnical University (Tomsk Polytechnic), Russia in 1977 and 1983, respectively. From 1977 to 1979 he worked as an Assistant Professor of electrical engineering at Tomsk Polytechnic. In 1978 he became involved in lightning research at the High Voltage Research Institute, a division of Tomsk Polytechnic, where from 1984 to 1994 he held the position of Director of the Lightning Research Laboratory. In 1985, Dr. Rakov received the rank of Senior Scientist in High Voltage Engineering. He has been named an Inventor of the USSR (1986) and received a Silver Medal from the (USSR) National Exhibition of Technological Achievements (1987). In 1991, he joined the faculty of the Department of Electrical and Computer Engineering at UF. Dr. Rakov is Chairman of the Technical Committee on Lightning of the biennial International Zurich Symposium on Electromagnetic Compatibility. Additional information is found at http://plaza.ufl.edu/rakov.

Martin A. Uman is Professor and Chair of the University of Florida's Department of Electrical and Computer Engineering. Dr. Uman has written 3 books on the subject of lightning, as well as a book on plasma physics, ten book chapters and encyclopedia articles on lightning, and has published over 140 papers in reviewed journals. He holds 5 patents, 4 in the area of lightning detection. Dr. Uman received the Ph.D. degree from Princeton University in 1961. He was an Associate Professor of electrical engineering at the University of Arizona in Tucson from 1961 to 1964. Dr. Uman joined the University of Florida faculty in 1971 after working for seven years as a Fellow Physicist at Westinghouse Research Labs in Pittsburgh. Dr. Uman co-founded and served as President of Lightning Location and Protection Inc. (LLP) from 1975 to 1985. Dr. Uman is the recipient of the 1996 IEEE Heinrich Hertz Medal for "outstanding contributions to the understanding of lightning electromagnetics and its application to lightning detection and protection." Dr. Uman is a Fellow in three professional organizations: the American Geophysical Union (AGU), the American Meteorological Society (AMS), and the Institute of Electrical and Electronics Engineers (IEEE). A full biography is found at http://www.ece.ufl.edu.